Inverse Problems 4 (1988) 867–876. Printed in the UK

Tomographic reconstructions from incomplete data—numerical inversion of the exterior Radon transform

Eric Todd Quinto

Department of Mathematics, Tufts University, Medford, MA 02155, USA

Received 23 December 1987

Abstract. X-rays passing through the beating heart or bone can create error in standard computer tomographic scans of the organs around these regions. Often doctors are interested in imaging only the organs surrounding these regions, not the regions themselves. The author's algorithm reconstructs the organs around the heart or metal without using the x-rays that create the error. Reconstructions of mathematical phantoms using this algorithm are given, and a description of the completed algorithm is presented. A mathematical explanation is given for the difficulties inherent in any tomography problem with incomplete data. It predicts weaknesses inherent in all reconstruction algorithms that use incomplete data.

1. Introduction

In this article we present our algorithm to solve the mathematical problem of reconstructing a function defined outside a region in $\mathbb{R}^2$ from integrals over lines not intersecting that region, that is to invert the *exterior Radon transform*, R. The hole theorem (Cormack 1963, 1964, Helgason 1965, Ludwig 1966) asserts that this problem has a solution for functions of compact support, the densities that occur in practice. Reconstructions from the algorithm are given in §5.

There are a number of compelling practical reasons for such an algorithm. The mathematical problem in x-ray tomography is to recover a function in the plane—the density of a planar cross section of the body—from values of its integrals over lines in that plane (Natterer 1986). If the planar cross section intersects the heart, movement of the heart will create blurring in the reconstruction of that section (Shepp and Kruskal 1978 p 425). X-rays passing through metal or bone can create errors in standard computer tomographic scans of the organs around these objects by their large density and a physical phenomenon called beam hardening (Smith *et al* 1977). In both cases it is important to be able to get good reconstructions of the organs around these regions. X-rays that *do* pass through the region—x-rays *not* used by our algorithm—*are* corrupted by the region (e.g., by the movement of the heart or high density of metal in bone). X-rays that do *not* go through the region—x-rays used by our algorithm—are *not* corrupted. Therefore our algorithm will reconstruct the area around the heart or bone without using the corrupted data. This problem is also of interest in astronomical studies of the corona of the sun (Altschuler 1979) and in industrial tomography.

0266-5611/88/030867+10 $02.50

The standard algorithms (Natterer 1986) do not solve this problem. They need 'complete' data, including data over x-rays through the region (heart or bone), even to reconstruct the organs outside the region. As with other limited-data problems (Davison 1983, Louis 1986), this problem is much more highly ill-posed (that is, much more difficult and more sensitive to noise) than standard tomography. One reason is that there are 'null functions', satisfying $Rf_N = 0$, that are 'almost' of compact support. The existence of these functions complicates the reconstruction problem, even for functions of compact support (Shepp and Kruskal 1978, p 426). Moreover, examples (Finch 1985) can be used to show the inverse to the exterior transform is continuous in no range of Sobolev norms. Therefore inversion of this transform for functions of compact support is much more unstable than inversion of R with complete data (whose inverse is continuous of order $+\frac{1}{2}$ in Sobolev norms).

Our mathematical solution uses a singular value decomposition, theorem 3.2 (Perry 1977, Quinto 1983 for $\mathbb{R}^n$), that reconstructs a function defined outside the disc up to a null function. Because of the ambiguity created by the null functions, this is not an inversion method. Our key refinement is an algorithm to get rid of this ambiguity and to exactly reconstruct compactly supported functions.

Cormack (1963) developed an inversion method for the exterior transform using integral equations, but the numerical results are not good (Cormack 1979, see also Hansen 1981), but Lewitt and Bates (1978a, b) and Natterer (1980) give algorithms that are numerically better.

For mathematical reasons, the excluded region in all of these algorithms, the set over which data are not taken, is assumed to be a disc. However, any inversion algorithm for circular excluded regions can be adapted to elliptical excluded regions, $(x/a)^2 + (y/b)^2 \leqslant 1$, by linear transformation $(x, y) \rightarrow (x/a, y/b)$ with appropriate multiplicative factors for the line integrals.

Section 2 of this article provides the definitions and §3 gives the singular value decomposition. Section 4 gives the inversion procedure and the numerical algorithm, and in §5 are reconstructions from the algorithm plus an overview of the difficulties of limited-data reconstruction that predicts algorithm defects.

2. Definitions

First let $\cdot$ denote the standard inner product on R^2; let $|\ |$ be the induced norm and let dx be Lebesgue measure on R^2. At the same time let $\theta \in [0, 2\pi]$ and let $p \in R$. Now let $d\theta$ and dp denote the standard measures on $[0, 2\pi]$ and R, respectively. In order to define the Radon transform let $L(\theta, p) = \{x \in R^2 | x \cdot \bar{\theta} = p\}$, the line with normal vector $\bar{\theta} = (\cos\theta, \sin\theta)$ and directed distance p from the origin. The points (θ, p) and $(\theta + \pi, -p)$ parametrise the same line $L(\theta, p)$. Therefore we will always assume $p \geqslant 0$ in this article. Let dx_L be arc length, the measure on $L(\theta, p)$ induced from Lebesgue measure on R^2.

The classical Radon transform is defined for an integrable function f on R^2 by

$$Rf(\theta, p) = \int_{L(\theta, p)} f(x)\, dx_L. \tag{2.1}$$

$Rf(\theta, p)$ is just the integral of f over the line $L(\theta, p)$.

Let E be the exterior of the unit disc in R^2, $E = \{x \in R^2 | 1 \leqslant |x|\}$, and let $E' = [0, 2\pi] \times [1, \infty)$. E' corresponds to the set of lines $L(\theta, p)$ that are contained in E.

The *exterior Radon transform* is the transform R as a map from integrable functions on E to integrable functions on E'. The problem posed in the first sentence of this article, recovering a function defined outside a disc from integrals over lines not intersecting that disc, is solved by inverting the exterior Radon transform.

The following spaces of functions will be used in §3. Let $L^2(E)$ be the Hilbert space of functions on E defined by the inner product

$$\langle f_1, f_2\rangle_E = \frac{1}{\pi}\int_E f_1(x)\overline{f_2(x)}|x|(1-|x|^{-2})^{1/2}\,dx \tag{2.2}$$

and let $L^2(E')$ be the Hilbert space of functions on E' defined by the inner product

$$\langle g_1, g_2\rangle_{E'} = \frac{1}{\pi}\int_{E'} g_1(\theta,p)\overline{g_2(\theta,p)}p^{-1}\,d\theta\,dp. \tag{2.3}$$

Any function $f\in L^2(E)$ can be decomposed uniquely

$$f(r\bar{\theta}) = \sum_{l\in\mathbb{Z}} f_l(r)e^{il\theta} \tag{2.4}$$

where

$$f_l(r) = \frac{1}{2\pi}\int_0^{2\pi} f(r\bar{\theta})e^{-il\theta}\,d\theta \tag{2.5}$$

and $f_l\in L^2([1,\infty),\ (1/\pi)r^2(1-r^{-2})^{1/2}dr)$. For similar reasons each $g\in L^2(E')$ can be written uniquely as

$$g(\theta,p) = \sum_l g_l(p)\,e^{il\theta} \tag{2.6}$$

where g_l is defined in a manner analogous to (2.5) and $g_l\in L^2([1,\infty),\ (1/\pi)p^{-1}dp)$.

3. A singular value decomposition for the exterior Radon transform

In this section we give the singular value decomposition (SVD) for the exterior transform on the Hilbert spaces $L^2(E)$ and $L^2(E')$. First the bases are given (proposition 3.1) and then the SVD is given (theorem 3.2).

The bases will be expressed in terms of the following shifted Jacobi polynomials. Let $Q_m(\alpha,\beta,t)$ be the real-valued polynomial of degree m in t for $\alpha>-1$, $\beta>-1$, $m=0,1,2,\ldots$ such that $\{Q_m(\alpha,\beta,t)\}$ is an orthonormal basis of $L^2([0,1], t^\alpha(1-t)^\beta dt)$; specifically we require

$$\int_0^1 t^m Q_m(\alpha,\beta,t)t^\alpha(1-t)^\beta\,dt>0 \tag{3.1}$$

and

$$\int_0^1 Q_m(\alpha,\beta,t)\,Q_M(\alpha,\beta,t)t^\alpha(1-t)^\beta\,dt=\delta_{mM} \tag{3.2}$$

where the Kronecker delta, δ_{mM}, is equal to one if $m=M$ and is zero otherwise. Some properties of the Q_m are given by Perry (1977). They are related to the standard Jacobi polynomials by the formula $Q_m(\alpha, \beta, t)=(2^{1+\alpha+\beta}/h_m^{(\beta,\alpha)})^{1/2}P_m^{(\beta,\alpha)}(2t-1)$ where $h_m^{(\beta,\alpha)}$ is given in (4.3.3) of Szegö (1939).

Proposition 3.1. Let $m=0, 1, 2,\ldots$ and $l\in\mathbb{Z}$. The functions f_{lm} defined for $x\in E$ by

$$f_{lm}(r\bar{\theta})=r^{-2}Q_m(-0.5, 0.5, r^{-2})\,e^{il\theta} \tag{3.3}$$

for l even and

$$f_{lm}(r\bar{\theta})=r^{-3}Q_m(0.5, 0.5, r^{-2})\,e^{il\theta} \tag{3.4}$$

for l odd form an orthonormal basis of $L^2(E)$. The functions g_{lm} defined for $(\theta, p)\in E'$ by

$$g_{lm}(\theta, p)=p^{-1-l}Q_m(l, 0, p^{-2})\,e^{il\theta} \tag{3.5}$$

form an orthonormal basis of $L^2(E')$ where the orthonormal polynomials $Q_m(\alpha, \beta, t)$ are defined by (3.1) and (3.2).

For $t\in R$ we let $[t]$ denote the greatest integer that is less than or equal to t. We can now state the SVD.

Theorem 3.2. The exterior Radon transform $R:L^2(E)\to L^2(E')$ defined by (2.1)–(2.3) satisfies

$$Rf_{lm}(\theta, p)=0 \qquad \text{for} \qquad m<[|l|/2] \tag{3.6}$$

and

$$Rf_{lm}(\theta, p)=R_{lm'}g_{lm'}(\theta, p) \qquad \text{for} \qquad m\geq[|l|/2] \tag{3.7}$$

where $m'=m-[|l|/2]$ and

$$R_{lm'}=\frac{\sqrt{2\pi}}{\sqrt{|l|+2m'+1}}. \tag{3.8}$$

This theorem is R M Perry's decomposition for the exterior Radon transform on R^2 and is proved using identities given by Perry (1977) involving the Q_m. This is *not* an inversion method because of the presence of the non-trivial null space (3.6). Given the density, f, of a cross section of the body, and any null function, f_N, $R(f+f_N)=Rf$. That is, f, the accurate reconstruction, and $f+f_N$, an inaccurate one, give the same data, Rf. Thus, any reconstruction algorithm needs more information than the SVD to distinguish f from $f+f_N$. The SVD is generalised by Quinto (1983) to the Radon transform integrating over hyperplanes in $\mathbb{R}^n$, and the author's basic inversion method is outlined there.

Because the R_{lm} converge to zero as $|l|+m\to\infty$, we have

Corollary 3.3. $R:L^2(E)\to L^2(E')$ is a compact operator.

Some of the functions and constants in this section are related to those of Perry (1977). Our polynomials $Q_m(\alpha, \beta, t)$ are Perry's $Q_m^*(\alpha, \beta, t)$; our functions f_{lm} correspond to Perry's $f_{mn}^{1/2}$, where our l is equivalent to Perry's m, and our m is Perry's n. Finally, our R_{lm} is Perry's $R_{mn}^{1/2}$. The above theorems are true for other weighted L^2

spaces as proved by Perry (1977) and Quinto (1983). The specific spaces of (2.2)–(2.3) are used because they are numerically convenient.

4. The numerical inversion algorithm

The singular value decomposition and the null space characterisation, corollary 4.1, are now used to give an exact inversion method for functions of compact support. The mathematical ideas are now described, and the numerical algorithm is outlined.

Let $f(x) \in L^2(E)$ be the density to be reconstructed, and let $Rf(\theta, p) = \Sigma_{lm} d_{lm} g_{lm}(\theta, p)$. Then, the SVD gives part of the orthogonal expansion of f, namely,

$$f_R = \sum_{lm} (d_{lm}/R_{lm}) f_{l(m+|l/2|)}, \tag{4.1}$$

which is the projection of f onto the orthogonal complement of the null space of the exterior transform. Because $R_{lm} = O((|l| + m)^{-1/2})$, this procedure is only as mildly ill-posed as inversion of the Radon transform with complete data (compare with the singular values of Cormack (1964)). Now $f = f_R + f_N$, where f_N, the projection of f onto the null space of the exterior transform, is not recovered by the SVD.

By the nature of the singular value decomposition, (3.3), (3.4), (3.6), and the continuity of the exterior transform we have:

Corollary 4.1. A function $f_N \in L^2(E)$ is in the null space of $R: L^2(E) \to L^2(E')$ *iff* its lth polar Fourier coefficient, $(f_N)_l(r)$, is a polynomial in $1/r$ of the same parity as l, of degree less than l, and with lowest order term in $1/r$ of degree at least two.

This corollary is one of the keys to our inversion method. Its generalisation was proven for the Radon transform on $\mathbb{R}^n$ by Quinto (1982).

The other key is the simple but useful observation that all objects f that are of interest in x-ray tomography have known compact support. So, given the function f to be reconstructed, there is an *a priori* known radius K such that

$$f(x) = 0 \qquad \text{for} \qquad |x| \geq K. \tag{4.2}$$

Therefore

$$f_N(x) = -f_R(x) \qquad \text{for} \qquad |x| \geq K. \tag{4.3}$$

Corollary 4.2. If f satisfies equation (4.2), then (4.3) uniquely determines $f_N(x)$ for $x \in E$, (that is $|x| \geq 1$).

Proof. Assume f_N is in the null space of R, $f_N(x)$ is zero for $|x| \geq K$, and Rf_N is zero on E'. Then by corollary 4.1 and by hypothesis, for each l, $(f_N)_l(r)$ is a polynomial in $1/r$ that is zero on $[K, \infty)$ and hence zero on $[1, \infty)$. This proves the corollary.

The basic algorithm to recover f is to use equation (4.1) to recover $f_R(x)$, and then use equation (4.3) and the restriction of corollary 4.1 to find $f_N(x)$. By corollary 4.2, equation (4.3) uniquely determines $f_N(x)$ for all $x \in E$. As noted above, the reconstruction of f_R is about as stable as inversion of the Radon transform with complete data. The unstable part of the algorithm is the recovery of f_N.

Because the basis functions are expressed in terms of trigonometric monomials, the algorithm will be described on Fourier coefficients. Let $l \in \mathbb{Z}$, and let f_l be the coefficient to be recovered. Equation (4.1) gives $(f_R)_l(r)$. Then the algorithm solves for $(f_N)_l(r)$ for $r \geq 1$ using the *a priori* information (4.3) and corollary 4.1:

$$(f_N)_l(r) = -(f_R)_l(r) \qquad \text{for} \qquad r \geq K. \tag{4.4}$$

$$(f_N)_l(r) \text{ is a polynomial in } 1/r \text{ of degree less than } l \text{ for } r \geq 1. \tag{4.5}$$

(Also, $(f_N)_l(r)$ is of the same parity as l and has lowest order term of order two or three in $1/r$.) A polynomial of degree less than $|l|$ as in (4.5) is least-squares fit to the data, $-(f_R)_l(r)$, for $r \geq K$. This polynomial, the reconstruction for $(f_N)_l$, is extrapolated to $r \geq 1$ using the explicit knowledge of its coefficients. Finally,

$$f_l(r) = (f_N)_l(r) + (f_R)_l(r) \qquad \text{for} \qquad r \geq 1 \tag{4.6}$$

is the reconstruction of f_l.

The numerical implementation of the least-squares fit is as follows. A constant $K_1 > K$ is chosen, and the function $(f_N)_l$ is found by a least-squares projection of $-(f_R)_l(r)$ for $r \geq K_1$ onto the null space (low-degree polynomials in $1/r$) for $r \geq K_1$. Then the projection is extrapolated to $r \geq 1$ using the special nature of the null space (4.5). Experimentally, optimal values of K_1 are known, depending on K (K_1 is chosen greater than K because of the Gibbs phenomenon in the recovery of $(f_R)_l$ near $r = K$). This extrapolation method is fairly insensitive to noise but only works well for small $|l|$; for large $|l|$ the extrapolated function blows up near $r = 1$ because, in general, extrapolation of high-degree polynomials is highly unstable.

An improvement is used for larger l that 'pins down $(f_N)_l(r)$ near $r = 1$'. *Choose* a constant a_l and *assume* the value of $f_l(r) = a_l$ for $r \simeq 1$. Then

$$(f_N)_l(r) = a_l - (f_R)_l(r) \qquad \text{for} \qquad r \simeq 1. \tag{4.7}$$

The improved numerical method to find $(f_N)_l$ is: solve for $(f_N)_l$ using (4.4) and (4.7) with constraint (4.5) and interpolate to find $(f_N)_l(r)$ for $r \geq 1$.

The extrapolation of the original method is turned into a more stable interpolation procedure. A least-squares projection is done onto the null space, (4.5), with nodes $r \simeq 1$ and $r \geq K_1$ and specified weights. Then the solution, $(f_N)_l$, is interpolated between $r \simeq 1$ and $r \geq K_1$. In some cases a_l is known explicitly. When not, an error estimate for the solution *at the nodes* can be used to find a good approximation to a_l. In many cases, the proper value of a_l is close to a local minimum of the error estimate of the solution in (4.4) and (4.7) as a function of a_l. Also, in all cases *a priori* bounds are known: $|a_l| \leq \sup_{r \simeq 1} f_0(r)$ where f_0, the zeroth Fourier coefficient of f, is known exactly as the null space is $\{0\}$ for $l = 0$. For large l near the limit of the algorithm, the error estimate does not work; high-degree polynomials can approximate data for any a_l. For such l, a_l is set to zero. For accurate a_l, the more nodes there are near 1, the more coefficients are recovered. For an inaccurate guess of a_l, the error between the reconstruction and the object being reconstructed decreases more rapidly for $r \gg 1$ if fewer nodes are used near $r \simeq 1$.

5. Reconstructions and analysis

As can be seen from the reconstructions of figures 1 and 2, the greatest reconstruction error occurs near $r = 1$. The reconstructions show that, in general, the closer K is to 1,

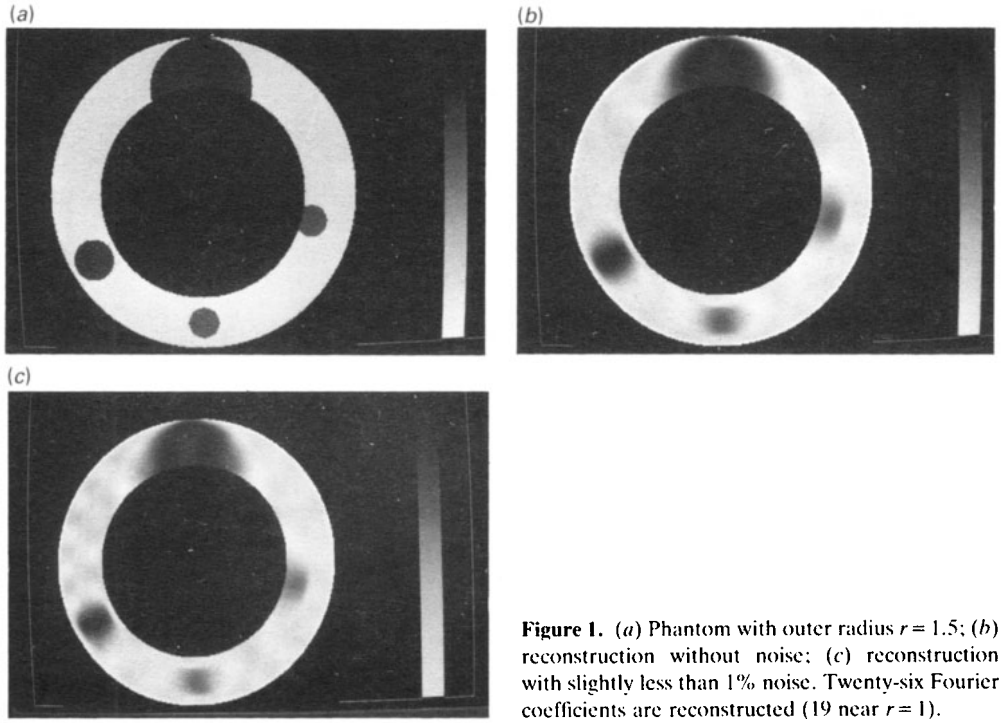

Figure 1. (*a*) Phantom with outer radius $r = 1.5$; (*b*) reconstruction without noise; (*c*) reconstruction with slightly less than 1% noise. Twenty-six Fourier coefficients are reconstructed (19 near $r = 1$).

the better the reconstruction. This is because the smaller K is, the shorter distance f_N needs to be extrapolated or interpolated.

Figure 1(*a*) is a phantom with outer radius $K = 1.5$. The two bigger circles have density 1.5 and the two smaller 1.375. Figure 1(*b*) is the reconstruction without noise, and figure 1(*c*) is the reconstruction with slightly less than 1% L^∞ noise. Twenty-six Fourier coefficients (19 near the inner boundary, $r = 1$) and 130 polynomials in $1/r$ are reconstructed using 100 values of p and 256 of θ.

Figure 2(*a*) is a phantom with outer radius $K = 2$. Again, the two bigger circles have density 1.5, the two smaller 1.375, the surrounding material has density 1. Figure 2(*b*) is the reconstruction without noise, and figure 2(*c*) is the reconstruction with slightly less than 1% L^∞ noise. Twenty-two polar Fourier coefficients (16 near the inner boundary) and 130 polynomials in the radial direction are reconstructed using 150 values of p and 256 values of θ. The convolution used for $r = 2$ smooths more than the convolution used for $r = 1.5$. These reproductions do not show as much contrast between density values of 1.3 to 1.5 as the original reconstructions do. Thus, the small circles look less round and closer to each other in density than in the originals.

These phantoms were chosen to be hard for my method—the high Fourier coefficients near the hole are *not* zero, even though my algorithm sets them to zero ($a_l = 0$ for large $|l|$). These phantoms are comparable in difficulty to others in the literature of this problem (Lewitt and Bates 1978a, b, Natterer 1980).

The side boundaries of each circle (where θ varies) are less precisely reconstructed than the outside and inside boundaries (where r varies). This reflects the fact that many more polynomials in the radial direction can be used than Fourier coefficients in θ.

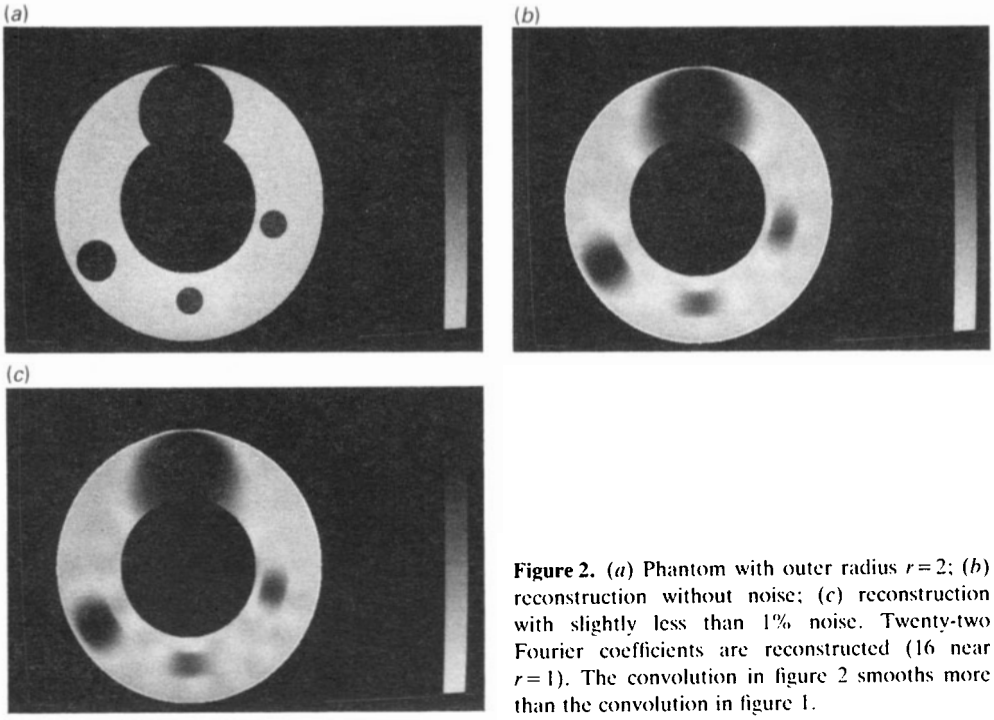

Figure 2. (*a*) Phantom with outer radius $r=2$; (*b*) reconstruction without noise; (*c*) reconstruction with slightly less than 1% noise. Twenty-two Fourier coefficients are reconstructed (16 near $r=1$). The convolution in figure 2 smooths more than the convolution in figure 1.

This can be understood in terms of an analytic property of R. An object, f, to be reconstructed consists of a cross section of the body, several regions, (e.g., brain, bone, cranial fluid) with well defined boundaries. A reconstruction is good if it precisely shows the boundaries. In limited-data tomography, the data set (lines over which data are taken) is not evenly distributed. (A data set is evenly distributed if, near each point in the cross section, there are lines in many directions that are 'uniformly distributed').

The key idea that predicts reconstruction inaccuracies is:

> The Radon transform detects boundaries of f that are tangent to lines being integrated over, but not boundaries in other directions. (5.1)

For a simple illustration, let $f(x)$ be 1 if $|x|\leq 1$ and 0 otherwise. For any θ, $Rf(\theta, p)=2(1-p^2)^{1/2}$ if $|p|\leq 1$ and zero otherwise. For $p\neq 1$, $Rf(\theta, p)$ is smooth. Exactly at the lines tangent to the boundary of f, $L(\theta,\pm 1)$, $Rf(\theta, p)$ is not smooth (the first derivative is infinite). If, as in limited-angle tomography, θ is restricted, say $\theta\in(-\pi/4, \pi/4)$, then (5.1) claims that the side boundaries of f should be detected well by the data, but the top and bottom boundaries should be less clearly seen. Boundaries tangent to lines in the data set are easy to detect because the data, Rf, have a jump in the first derivative there. Boundaries not tangent to lines in the data set should be harder to 'see'. A good reconstruction algorithm for a limited-data problem should, therefore, reconstruct boundaries tangent to lines in the data set much more clearly than boundaries *not* tangent to lines in the data set. Boundaries not tangent to lines in the data set should be more blurred.

This phenomenon is seen in all the reconstructions in figures 1 and 2. The outside and inside boundaries of the small circles—boundaries tangent to lines in the data

set—are detected more clearly by the algorithm than the side boundaries—those not tangent to lines in the data set. The inside boundaries only intersect a few lines in the data set, but because they intersect tangentially, they are more clearly defined. The reconstructions of Lewitt and Bates (1978) and Natterer (1980) for the exterior problem have similar distortions at boundaries.

This phenomenon is also seen in the singular functions for limited-angle tomography (see Louis (1986) for pictures). Singular functions corresponding to large singular values (functions that are easier to reconstruct) oscillate perpendicular to lines in the data set. The given data easily detect these oscillations. Singular functions corresponding to small singular values (harder to reconstruct) oscillate *parallel* to (that is along) lines in the data set. These functions are harder to reconstruct, because their oscillations are not detected well by the given data. (Similarly, the null functions for the exterior problem oscillate less in p—that is perpendicular to lines in the data set for the exterior problem—than in θ).

This general phenomenon has been observed by many researchers. For example, it is the tangent casting of Shepp and Srivastava (1986). It is the idea behind the ill-posedness proof of Finch (1985).

The rigorous mathematical reason for (5.1) is that R is an elliptic Fourier integral operator that detects singularities when the singularities are perpendicular to the line being integrated over but not otherwise (if $Rf(\theta, p)$ is not smooth for all (θ, p) near (θ_0, p_0), then for some $x \in L(\theta_0, p_0)$, f is not smooth at x in direction θ_0 (that is, $(x, \theta_0) \in (WF(f))$ and conversely, if $Rf(\theta, p)$ is smooth near (θ_0, p_0), then for all $x \in L(\theta_0, p_0)$, f is smooth at x in direction θ_0 (that is, $(x, \theta_0) \notin WF(f)$]. (See e.g. Quinto (1980) for the Lagrangian manifold calculation from which one discovers how R detects singularities and Treves (1980) for general information). The singularities involved are numerically meaningful because they are discontinuities in the first derivative. Frank Natterer has proposed a heuristic explanation of this phenomenon using Radon's inversion formula and the observation that Rf is generally discontinuous in the first derivative at boundaries. Similar arguments help explain why lambda tomography (Smith and Keinert 1985) works; $\Delta R^* R$ is an elliptic pseudo-differential operator and thus preserves singularities of f.

Acknowledgments

This research was supported by NSF grant 8701415 as well as by PHS research grant CA 32743 awarded by the US National Cancer Institute, DHHS. The author also thanks the West German Humboldt Foundation for a fellowship under which some of this mathematics was developed. Finally the author is deeply indebted to Alfred Louis, Frank Natterer and Don Solmon for their invaluable advice, as well as to Sarah Anderson, George Cybenko, David Krumme, Jon Polito and Bill Schlesinger for their practical help. We thank Allan Cormack for his constant support as well as for suggesting this problem.

References

Altschuler M D 1979 Reconstruction of the global-scale three-dimensional solar corona *Image Reconstruction from Projections, Implementation and Applications* ed. G T Herman (*Topics in Applied Physics* vol. 32) (Berlin: Springer) pp 105–45

Cormack A M 1963 Representation of a function by its line integrals with some radiological applications *J. Appl. Phys.* **34** 2722–7

—— 1964 Representation of a function by its line integrals with some radiological applications II *J. Appl. Phys.* **35** 2908–13

—— 1979 Private communication

Davison M 1983 The ill-conditioned nature of the limited angle tomography problem *SIAM J. Appl. Math.* **43** 428–48

Finch D V 1985 Cone beam reconstruction with sources on a curve *SIAM J. Appl. Math.* **45** 665–73

Hansen E W 1981 Circular harmonic image reconstruction: experiments *Appl. Opt.* **20** 2266–74

Helgason S 1965 The Radon transform on Euclidean spaces, compact two-point homogeneous spaces and Grassman manifolds *Acta Math* **113** 153–80

Lewitt R M and Bates R H T 1978a Image reconstruction from projections. II, Projection completion methods (theory) *Optik* **50** 189–204

—— 1978b Image reconstruction from projections. III, Projection completion methods (computational examples) *Optik* **50** 269–78

Louis A 1986 Incomplete data problems in x-ray computerized tomography 1. Singular value decomposition of the limited angle transform *Numer. Math.* **48** 251–62

Ludwig D 1966 The Radon transform on Euclidean space *Comm. Pure Appl. Math.* **19** 49–81

Natterer F 1980 Efficient implementation of 'optimal' algorithms in computerized tomography *Math. Meth. Appl. Sci.* **2** 545–55

—— 1986 *The Mathematics of Computerized Tomography* (New York: Wiley)

Perry R M 1977 On reconstructing a function on the exterior of a disc from its Radon transform *J. Math. Anal. Appl.* **59** 324–41

Quinto E T 1980 The dependence of the generalized Radon transform on defining measures *Trans. Am. Math. Soc.* **257** 331–46

—— 1982 Null spaces and ranges for the classical and spherical Radon transforms *J. Math. Anal. Appl.* **90** 408–20

—— 1983 The invertibility of rotation invariant Radon transforms *J. Math Anal. Appl.* **91** 510–22

Shepp L A and Kruskal J B 1978 Computerized tomography: the new medical x-ray technology *Am. Math. Monthly* **85** 420–39

Shepp L A and Srivastava S 1986 *Computed tomography of* PKM and AKM exit cones *A T & T Tech. J.* **65** 78–88

Smith K T and Keinert F 1985 Mathematical foundations of computed tomography *Appl. Opt.* **24** 3950–7

Smith K T, Solomon D C and Wagner S L 1977 Practical and mathematical aspects of the problem of reconstructing objects from radiographs *Bull. Am. Math. Soc.* **83** 1227–70

Szegö G 1939 *Orthogonal Polynomials* (Providence, RI: American Mathematical Society)

Treves F 1980 *Introduction to Pseudodifferential and Fourier Integral Operators* vols 1, 2 (New York: Plenum)